Characteristics of MERRA-2 Black Carbon in Eight Key Climatic Regions across China from 2007 to 2018

Yong Zhang[1], *Junli* Jin[1,*], *Yanan* Li[1], *Dajiang* Yu[2], *Qing* Zhou[1] and *Lina* Gao[1]

[1]Meteorological Observation Center, China Meteorological Administration, *Beijing, 100081 China*
[2]Longfengshan Atmospheric Background National Observation and Research Station, *Heilongjiang, 150200 China*

Abstract. The spatial distribution, temporal variations and trend changes of surface black carbon concentrations in eight key climatic regions across China were analyzed from 2007 to 2018 , based on the Modern-era Retrospective Analysis for Research and Applications Version 2 (MERRA-2) black carbon dataset. The mass concentration of BC in China shows an "East-High and West-Low" pattern, with multi-year averaged BC ranging from 154 ng/m^3 to 3857 ng/m^3. Pronounced seasonal variations were found, with the highest value in winter and the lowest in summer. Most of regions in central and eastern China share similar diurnal pattern with a single-peak at early morning and a valley at noon. Obvious downward trend in most regions of China were identified from 2007 to 2018, especially in southern central China and southwestern part of eastern China, with the highest decline rate of -8.349 ng/m^3 per month, which confirming that the great endeavors and effective enforcement of environmental protection measures implemented in China for the last decade.

1 Introduction

Black carbon (BC) is mainly produced by incomplete combustion of carbon-containing fuels and biomass burning[1]. Although BC only accounts for 5%-15% of urban aerosols[2], its ability to absorb sunlight accounts for 90%-95% of the total capacity of all absorbing aerosols[3]. In the Himalayan region, solar heating from BC at high elevations was considered to be equivalent to carbon dioxide in the melting of snow packs and glaciers [4]. Therefore, BC has been widely recognized as one of the most important climate agents of global warming[5]. Dozens of studies have been conducted to investigate the characteristics of BC combined with ground-based observations and satellite data[6-8], both of which have scientific limitations. For one hand, ground-based observations mostly reflect a small range of local characteristics, and the sparseness of the observation stations only make it difficult to study the large scale regional distributions. On the another hand, the satellite observations are usually affected by various factors such as clouds and atmosphere pollutions, leading to inaccurate estimates which are non-negligible in further research. Alternatively, 'data reanalysis' was proposed in recent years to assimilate data from different sources and types to form large-scale, uniformly distributed grid data, such as the BC product of Modern-Era Retrospective Analysis for Research and Applications, version 2 (MERRA-2)[9-10]. Given the robust data qualit, the application of MERRA-2 black carbon dataset can provide a better scientific understanding of characteristics of BC, like spatial distribution, temporal variation, vertical profiles and radiation balance globally. In East Asian, including China, BC is quite abundant in the atmosphere due to rapid industrialization and urbanization[11], as well as frequent biomass burning[12-13], leading to growing global attention. In this study, BC characteristics of eight key climatic regions across China are studied and highlighted in details.

2 Data description

The MERRA-2 is the atmospheric reanalysis datasets symbolizing a new modern satellite era (1980 onward), released by the NASA Global Modeling and Assimilation Office. It is produced with version 5 of the Goddard Earth Observing System Model (GEOS) atmospheric data assimilation system. The key components of the system are the GEOS atmospheric model and the Gridpoint Statistical Interpolation (GSI) meteorological analysis scheme[9].

The datasets of MERRA-2 include observable parameters and aerosol diagnostics not easily observed on a global scale, with a time resolution of 1h, 3h, and 1month and a horizontal resolution of 0.5° × 0.625° latitude by longitude grid. The vertical structure is divided to 72 hybrid-eta levels from the surface to 0.01 hPa. The MERRA-2 reanalysis products are currently publicly available online through the Goddard Earth Sciences Data and Information Services Center (http://disc.sci.gsfc.nasa.gov/mdisc/).

We here focused only on the BC surface mass concentration of MERRA-2 (BCSMASS), upon which the spatial distribution, temporal variations and trend

* Corresponding author: jinjl@cma.gov.cn

changes of BC concentration in eight key climatic regions of China were studied from 2007 to 2018.

3 Results and analysis

3.1 Spatial distribution of BC surface mass concentration

Figure 1 shows the spatial distribution of annual mean BCSMASS from 2007 to 2018. As is known, meteorological conditions have great influence on the concentration of aerosols. The BC concentration varies from one climatic region to another, also due to the significant geographic dependence of climatic characteristics in China. Here, we marked eight regions, namely Northeast (NEC), North China (NC), East China (EC), South China (SC), Central China (CC), Southwest (SWC), Northwest (NWC) and Qinghai-Tibet Plateau (TP), according to previous studies[14-15].

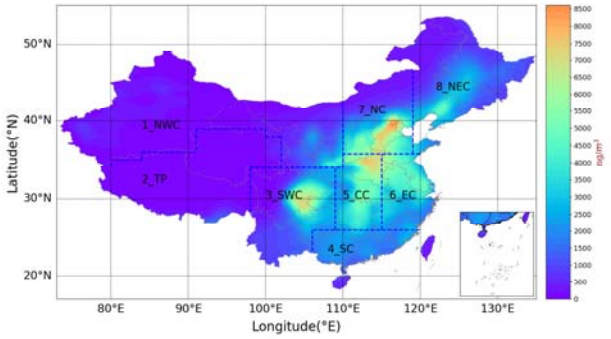

Fig. 1 Spatial distribution of mean BCSMASS across China from 2007 to 2018.The regions are numbered as follows, Northeast (NEC, region 8), North China (NC, region 7), East China (EC, region 6), South China (SC, region 4), Central China (CC, region 5), Southwest China (SWC, region 3), Northwest China (NWC, region 1) and Qinghai-Tibet Plateau (TP, region 2).

In general, the BCSMASS in China shows a featured pattern of "East-High and West-Low". The average concentration corresponding to the Northwest, Northeast, North China, East China, South China, Central China, Southwest, and Qinghai-Tibet Plateau key regions are 384 ± 543 ng/m^3, 1390 ± 959 ng/m^3, 2621 ± 2266 ng/m^3, 3324 ± 1290 ng/m^3, 1803 ± 487 ng/m^3, 3857 ± 1440 ng/m^3, 1759 ± 1725 ng/m^3, and 154 ± 253 ng/m^3, respectively. Please note that the relatively high standard deviation from the multi-year mean values in several regions was caused by strong fluctuations and differences in BC concentration from grid to grid and also day to day. The high BCSMASS, above 5000 ng/m^3, are mainly found in Hebei, Henan and Sichuan provinces, consistent with the results obtained by Zhang et al. (2019) based on in-situ observations[16] with reasonable differences in the concentration values. The vast western regions in China are characterized with low BC concentrations, reflecting obvious low BC emissions and less anthropogenic and industrial activities. A worth-noting region lies in NEC. The BC concentration in NEC region is high according to ground-based observations[17-18], comparable to the high concentration in the NC region. However, the BC concentration over NEC is relatively low from our study, which may indicate the underestimation of the MERRA-2 BC data in NEC region.

3.2 Seasonality of BC surface mass concentration

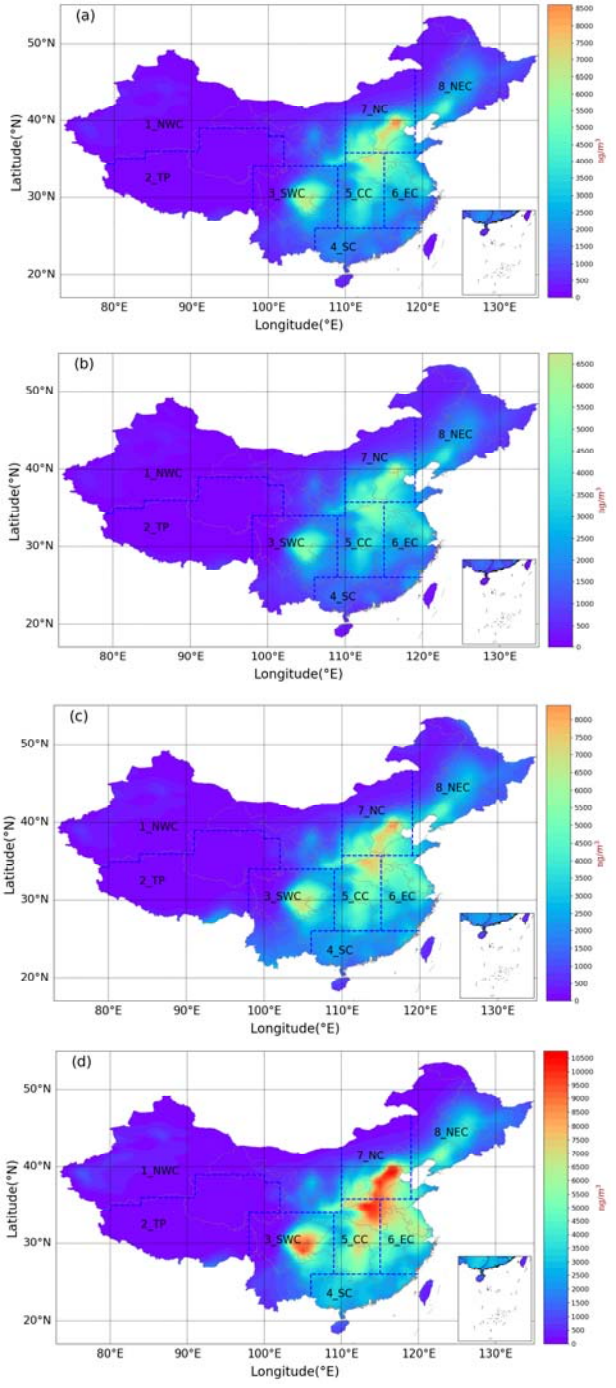

Fig. 2 Seasonal distributions of BCSMASS across China in (a) spring (MAM), (b) summer (JJA), (c) autumn (SON) and (d) winter (DJF) from 2007 to 2018.

Figure 2 shows the distributions of BCSMASS across China averaged over four seasons from 2007 to 2018. Pronounced seasonal variations of BC can be identified, with the highest concentration in winter, and then followed by spring and autumn. The lowest BC

concentration occurs in summer. The winter maxima and summer minima is typical seasonality of primary air pollutants in mid-latitudes area, and is in good agreement with research of a 1-year national-scale measurement in China[19]. The low concentration in summer is most likely attributed to no emissions from heating and stronger wet scavenging induced by East Asian Summer Monsoon precipitation[20]. The BCSMASS in NC, SWC, CC, and EC regions in winter are 3131±3035 ng/m^3, 2179±2364 ng/m^3, 5279±1941 ng/m^3 and 4643±1849 ng/m^3 respectively. And that of summer are 2215±1686 ng/m^3, 1325±1345 ng/m^3, 2833 ± 1120 ng/m^3 and 2514 ± 974 ng/m^3, respectively, showing apparent reductions. While in NWC and TP regions, the differences of averaged BC concentrations between winter and summer are 162 ng/m^3 and 22 ng/m^3, quite subtle in comparison with other key regions in central and eastern China.

3.3 Monthly variations of BC surface mass concentration

Figure 3 shows the averaged monthly variation of BCSMASS in eight key regions across China from 2007 to 2018. Generally speaking, the monthly mean BCSMASS peak in January or December, whereas the lowest BC concentration occur in summer months, varied from May to August, for most of key regions like NWC, SWC, SC, CC, EC and NC regions. Based on the analysis of MERRA-2 BC in eastern China (corresponding to the CC, EC, and southern regions of NC in our study) from 2008 to 2016, Xu et al. (2020) also found similar monthly variation pattern with high BC concentrations appearing in winter period and low BC concentrations occurring in the summer months [21].

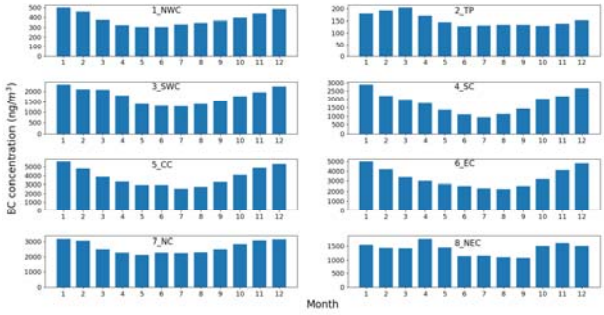

Fig. 3 Averaged monthly variation of BCSMASS in eight key regions across China from 2007 to 2018.

The main heating period in Northern China lasts from November to March of the following year, mainly covering the winter months. The increase in BC emissions from intensified coal combustion (transportation sector contributes as well), coupled with the frequent presence of unfavorite weather conditions such as temperature inversion and calm wind, prevent the horizontal and vertical dispersion and transportation of black carbon aerosols, resulting in high concentrations in winter months.

Interestingly, an inconsistent pattern can be spotted in the TP and NEC regions. The highest monthly average concentration occurs in March and the lowest monthly average concentration occurs in June in TP. While in the NEC region, monthly average concentrations remain at high level from late autumn to spring and reached at lower level in summer, generally consistent with its longer heating period. Previous researches conducted by Yang et al. (2018) and Ji (2018) indicated that South Asia, Central Asia, eastern China and the northern part of the Qinghai-Tibet Plateau accounted for 74.3% of the BC input into the TP region during the non-monsoon period[22-23]. While during the monsoon period, their total contributions reduced to 36%. The influence of external BC input from surrounding regions and the circulations of monsoon may be responsible for the slightly different variation pattern in TP region.

3.4 Diurnal variations of BC surface mass concentration

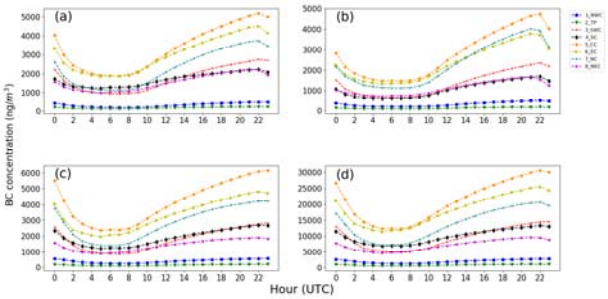

Fig. 4 Diurnal variations of BCSMASS in eight key climatic regions across Chinain (a) spring (MAM), (b) summer (JJA), (c) autumn (SON) and (d) winter (DJF) from 2007 to 2018.

Figure 4 presents the diurnal variations of BCSMASS in eight key regions in four seasons during the research period. The BC in winter is much higher than other seasons in all regions. The diurnal variation patterns of BC concentration can be divided into two groups for different regions. Firstly, most of regions in central and eastern China share similar diurnal pattern with a single-peak appearing at 22:00-23:00 UTC and a single-valley appear at 5:00-7:00 UTC, corresponding to early morning and noon period of local time in China. This diurnal variation pattern mainly indicates the importance of primary air pollutants accumulation during the night and dispersion or dilution of BC along with the development of boundary layer during the day. Secondly, the diurnal variations in TP and NWC are quite flat, showing daily BC minima. Zhang et al. (2019) demonstrated that most of the daily variation patterns of BC concentration in China (at 80% of the observation sites) were bimodal, with two peaks corresponding to two rush hours of the day. This divergence can be explained by the representativeness limitations of ground observations, which reflects the influence of fuel combustion (and cooking as well) around the observation sites during two rush hours. While these local features cannot be observed from MERRA-2 reanalysis, either regional or large-scale characteristics retain.

3.5 Trends in BC surface mass concentration

Figure 5 shows the spatial distribution of the trends in BCSMASS in eight key regions across China. Obviously, , the BCSMASS showed a downward trend in most regions of China from 2007 to 2018, especially in southern CC and southwestern part of EC regions, with the highest decline rate of -8.349 ng/m^3 per month in southeastern part of Sichuan province. The downward trend is consistent with and supported by ground-based black carbon observations across China from 2006 to 2017[16]. It is also in agreement with other researches indicating a decrease in black carbon absorption aerosol optical depth during 2008–2017 in China and a decrease in BC surface mass concentration in East China during 2008-2016[21, 24]. Series of trend analysis researches, including this work, have proved the fact of decrease in BC concentration in China in the recent decade, quite opposite to former trend prediction of BC emissions, which claimed a rapid growth in Asia from 1980 to 2020 [25]. This remarkable achievement has been attributed to the effective enforcement of environmental protection measures in China for around 10 years[26].

Please note that the slight increasing trends of BCSMASS in Heilongjiang province and the northwest of Xinjiang Autonomous Region have not been discussed because trends there did not pass the t-test at the 0.05 significance level.

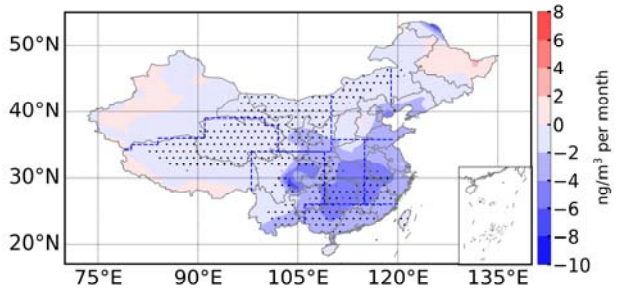

Fig. 5 The linear trend fitted for BCSMASS across China from 2007 to 2018 (Unit: ng/m^3 per month), the black dots denote the trends that passed the t-test at the 0.05 significance level.

4 Conclusions

Based on the MERRA-2 BC dataset, characteristics of spatial, seasonal distribution and temporal variations of BC surface mass concentration in eight key climatic regions across China were analyzed from 2007 to 2018. From high to low, the average concentration of BC in these eight key regions are 3857±1440 ng/m^3, 3324±1290 ng/m^3, 2621±2266 ng/m^3, 1803±487 ng/m^3, 1759±1725 ng/m^3, 1390±959 ng/m^3, 384±543 ng/m^3, and 154±253 ng/m^3, corresponding to the CC, EC, NC, SC, SWC, NEC, NWC, and TP regions respectively, with strong fluctuations and differences in BC concentration from grid to grid and also day to day.

The BCSMASS in China shows an "East-High and West-Low" pattern, in agreement with in-situ observations. Pronounced seasonal variations of BC were identified, with the highest concentration in winter the lowest in summer. The monthly mean BCSMASS peaks in January or December, whereas the lowest BC concentration occur in summer months, varied from May to August, for most of key regions in central and eastern China. This seasonality is typical among primary air pollutants and is attributed to the increase in BC emissions from intensified coal combustion and transportation, coupled with unfavorite weather conditions in the heating period. As for diurnal variation feature in 4 seasons, most of regions in central and eastern China share similar diurnal pattern with a single-peak at early morning and a valley at noon in local time, mainly indicate the importance of primary air pollutants accumulation during the night and dispersion or dilution of black carbon along with the development of boundary layer during the day. Obvious downward trend in most regions of China were identified from 2007 to 2018, especially in southern central China and southwestern part of eastern China, with the highest decline rate of -8.349 ng/m^3 per month in southeastern part of Sichuan province. This downward trend is consistent with and supported by ground-based BC observations across China for last decades, and this remarkable achievement has been attributed to the effective enforcement of environmental protection measures in our country.

Acknowledgment

This work was supported by the Ministry of Science and Technology of China under project No. 2017YFC1501802, the National Nature Science Foundation of China under project Nos. 41805027, 91644223. The authors appreciate the NASA Global Modelling and Assimilation Office for providing the MERRA-2 data online.

References

1. Bond T., D. Streets, K. Yarber, S. Nelson, J. H. Woo, Z. Klimont. A technology-based global inventory of black carbon emissions from combustion. J. Geophys. Res. Atmos. **109**, (2004)
2. Yang F., J. Tan, Q. Zhao, Z. Du, K. He, Y. Ma, F. Duan, G. Chen. Characteristics of $PM_{2.5}$ speciation in representative megacities and across China. Atmos. Chem. Phy. **11**, 5207–5219 (2011)
3. Hansen A., V. Kapustin, V. Kopeilin, D. Gillette, B. Bodhaine. Optical absorption by aerosols black carbon and dust in a desert region of central Asia. Atmos. Enciron. **27**, 2527–2531(1993)
4. Ramanathan V., G. Carmichael. Global and regional climate changes due to black carbon. Nature Geoscience, **1**(4): 221–227 (2008)
5. Bond T. C., S. J. Doherty, D. W. Fahey, P. M. Forster, T. Berntsen, B. J. DeAngelo. Bounding the role of black carbon in the climate system: a scientific assessment. J. Geophys. Res. Atmos. **118**, 5380–5552 (2013)
6. Yan P., J. Tang, J. Huang, J. Mao, X. Zhou, Q. Liu, Z. Wang, H. Zhou. The measurement of aerosol

optical properties at a rural site in Northern China. Atmos. Chem. Phys. **8**, 2229–2242 (2008)

7. Sharma M. C., V. K. Pandey, R. Kumar, S. U. Latief, E. Chakrawarthy, P. Acharya. Seasonal characteristics of black carbon aerosol mass concentrations and influence of meteorology, New Delhi (India). Urban Clim. **24**, 968–981 (2018)
8. Cohen J. B., Quantifying the occurrence and magnitude of the Southeast Asian fire climatology. Environ. Res. Lett. **9**, (2014)
9. Ronald G., W. McCarty, M. J. Suarez, et al. The Modern-Era Retrospective Analysis for Research and Applications, Version 2 (MERRA-2). J. Climate **30** (14): 5419–5454 (2017)
10. Randles C., A. Da Silva, V. Buchard, P. Colarco, A. Darmenov, R. Gocindaraju, A. Smirnov, B. Holben, R. Ferrare, J. Hair. The MERRA-2 aerosols reanalysis, 1980 onward. Part I: system description and data assimilation evaluation. J. Clim. **30**, 6823–6850 (2017)
11. Zhang R., G. Wang, S. Guo, M. L. Zamora, Q. Ying, Y. Lin. Formation of urban fine particulate matter. Chem. Rev. **115**, 3803–3855 (2015)
12. Huang J., J. Guo, F. Wang, Z. Liu, M. J. Jeong, H. Yu, Z. Zhang. CALIPSO inferred most probable heights of global dust and smoke layers. J. Geophys. Res. Atmos. **120**, 5085–5100 (2015)
13. Li Z., J. Guo, A. Ding, H. Liao, J. Liu, Y. Sun, T. Wang, H. Xue, H. Zhang, B. Zhu. Aerosol and boundary-layer interactions and impact on air quality. Natl. Sci. Rev. **4**, 810–833 (2017)
14. Zhang Y., Y. Xu, W. Dong, L. Cao, M.Sparrow. A future climate scenario of regional changes in extreme climate events over China using the PRECIS climate model. Geophys. Res. Lett. **33**, (2006)
15. Zhang Y., L. Gao, L. Cao, Z. Yan, Y. Wu. Decreasing atmospheric visibility associated with weakening winds from 1980 to 2017 over China, Atmos. Environ. **224**, (2020)
16. Zhang Y., Y. Li, J. Guo, Y. Wang, D. Chen, H. Chen. The climatology and trend of black carbon in China from 12 year ground observation, Climate Dyn. **53**, 5881–5892 (2019).
17. Gao Z., R. Zhang, L. Su. Characteristic analysis of atmospheric black carbon aerosols in Changchun in autumn and winter. Plateau Meteorology. **4**, 803–807 (2009)
18. Wang Y., Y. Ma, Z. Lu, D. Zhou, N. Liu, Y. Zhang, Y. Hong. In situ continuous observation of atmospheric black carbon aerosol mass concentration in Liaoning region. Reserch of Envornmental Sciences. **24**(10) : 1088–1096 (2011)
19. Cao J., S. C. Lee, J. C. Chow, J. G. Watson, K. F. Ho, R. Zhang, Z. Jin, Z. Shen, G. Chen, Y. Kang, S. Zou, L. Zhang, S. Qi, M. Dai, Y. Cheng, K. Hu. Spatial and seasonal distributions of carbonaceous aerosols over China. J. Geophys. Res. Atmos. **112**, (2007)
20. Li Z., W. K. M. Lau, V. Ramanathan, G. Wu, Y. Ding, M. G. Manoj et al. Aerosol and monsoon climate interactions over Asia. Rev. Geophys. **54**, 866–929 (2016)
21. Xu X., X. Yang, B. Zhu,Z. Tang, H. Wu, L. Xie. Characteristics of MERRA-2 black carbon variation in east China during 2000-2016. Atmos. Environ. **222**, (2020)
22. Yang J., S. Kang, Z. Ji, et al. Modeling the origin of anthropogenic black carbon and its climatic effect over the Tibetan Plateau and surrounding regions. J. Geophys. Res. Atmos. **123**(2): 671–692 (2018)
23. Ji Z. Advances and prospects of research on simulating transboundary black carbon and their climatic effects over the Tibetan Plateau. Progress in Geography. 37(4) : 465–475 (2018)
24. Sun E., X. Xu, H. Che, Z. Tang, K. Gui, L. An, C. Lu, G. Shi. Variation in MERRA-2 aerosol optical depth and absorption aerosol optical depth over China from 1980 to 2017. J. Atmos. Sol.-Terr. Phy. **186**, 8–19 (2019)
25. Ohara T., H. Akimoto, J. Kurokawa, N. Horii, K. Yamaji, X. Yan, T. Hayasaka. An Asian emission inventory of anthropogenic emission sources for the period 1980–2020. Atmos. Chem. Phys. **7**, 4419–4444 (2007)
26. Wang R., S.. Tao, W. Wang, et al. Black carbon emissions in China from 1949 to 2050. Environ. Sci. Technol. **46**(14) : 7595–7603 (2012)